Topological Hall Effect in Pyrochlore Lattice with Varying Density of Spin Chirality

K. Ueda,[1] S. Iguchi,[1,*] T. Suzuki,[2] S. Ishiwata,[1] Y. Taguchi,[2] and Y. Tokura[1,2,3]

[1]*Department of Applied Physics, University of Tokyo, Tokyo 113-8656, Japan*

[2]*Cross-Correlated Materials Research Group (CMRG) and Correlated Electron Research Group (CERG), RIKEN Advanced Science Institute (ASI), Wako 351-0198, Japan*

[3]*Multiferroics Project, ERATO, Japan Science and Technology Agency (JST), Tokyo 113-8656, Japan*

(Received 29 October 2011; published 9 April 2012)

The three-site spin correlation, $\boldsymbol{S}_i \cdot (\boldsymbol{S}_j \times \boldsymbol{S}_k)$ on the neighboring triangular sites i, j and k, termed scalar spin chirality, can endow the conduction electron with a quantum Berry phase and resultant transverse (Hall) transport. The paramagnetic barely metallic state was prepared in hole-doped $Y_2Mo_2O_7$ with pyrochlore lattice using a high-pressure synthesis method, which is further endowed with the spin chirality by partially replacing Y site with Tb (content x). The local spin chirality formed by the adjacent three Tb Ising moments on the pyrochlore lattice can couple to the conduction electrons to give rise to the topological Hall effect whose magnitude increases in proportion to x^3 or the density of the Tb-moment triangular clusters.

DOI: 10.1103/PhysRevLett.108.156601 PACS numbers: 72.15.Gd, 72.25.Ba, 75.25.−j, 75.30.−m

Topological spin textures in solids can be a source of emergent electromagnetic fields acting on the electron system, thereby generating versatile intriguing magneto-electronic phenomena [1]. One such example is the multiferroic state as ubiquitously realized in the transverse helical spin structure with the vector spin chirality ($\boldsymbol{S}_i \times \boldsymbol{S}_j$, i and j being the neighboring spin sites along the propagation direction) [2,3]. Another good example is the topological Hall effect as induced by the scalar spin chirality which endows the conduction electron with the quantum Berry phase. Here, the scalar spin chirality is defined as the three-spin correlation, $\chi_{ijk} = \boldsymbol{S}_i \cdot (\boldsymbol{S}_j \times \boldsymbol{S}_k)$ on the neighboring spin-triad i, j and k. The conduction electron whose spin is coupled with the background local spins forming the spin chirality may experience the complex value of transfer interaction whose phase factor is proportional to χ_{ijk}. The fictitious magnetic field (Berry curvature) caused by the Berry phase may induce a nontrivial Hall motion of the conduction electron as termed topological Hall effect (THE) [4–9].

The effect of Berry phase due to spin chirality is frequently canceled out by the sum over the whole lattice sites in real materials. However, when there are inequivalent multiple loops in a magnetic unit cell, the Berry phase curvature in the momentum space becomes nonzero with a possible finite Chern number of each band [6,10]. The topological Hall effect induced by this mechanism has been observed for pyrochlore-structure compounds $Nd_2Mo_2O_7$ [11,12] and $Pr_2Ir_2O_7$ [13], which certainly have two inequivalent loops (hexagons and triangles) in the pyrochlore-lattice unit cell. In this case, the THE is described by the same theoretical scheme as in the case of the intrinsic anomalous Hall effect (AHE) in which the spin-orbit interaction can give rise to the Berry curvature in the momentum space as well. The other contrastive view is due to the spin texture hosting the spin chirality, whose size is larger than the lattice constant or the electron mean free path (l). In this case, the spin chirality can give rise to the real-space Berry curvature, viewed as the local effective (fictitious) field acting on the hopping electrons around the spin-chiral sites [5]. One such example is a topological spin texture called skyrmion, in which the varying direction of the spins wraps a sphere [14–18]. In the continuum limit, the total spin chirality is proportional to the number of the skyrmion. The electron moving over the skyrmion spin texture acquires the Berry phase proportional to the skyrmion density [16–18]. Here, we present another generic case for the valid real-space picture, where the diffusive motion of the conduction electron with the mean free path being comparable with the lattice constant is interacting with the randomly distributed local spin chirality as defined by the atomic-size spin triad. In this study, such a situation is realized in barely metallic pyrochlores $(Y_{1-x-y}Tb_xCd_y)_2Mo_2O_7$, as derived from a Mott insulator $Y_2Mo_2O_7$ by doping holes and Tb Ising moments on the pyrochlore A-sites. The hole doping via the chemical substitution of Y^{3+} with Cd^{2+} ions produces the paramagnetic metallic state near the Mott transition, in which the diffusive-motion carriers are coupled with the Tb-moment triad forming spin chirality.

The pyrochlore $R_2Mo_2O_7$ (R being the trivalent rare-earth ion, Fig. 1(a)] is composed of two sublattices (both pyrochlore lattices) for R (so-called A sites) and Mo (B sites) which are, respectively, displaced by a half unit cell. A family of $R_2Mo_2O_7$ locates near the metal-insulator boundary [see Fig. 1(b)] because of the Coulomb correlation of Mo 4d electrons; the two 4d electrons in nominally Mo^{4+} state are accommodated in t_{2g} states, one itinerant in e'_g and the other localized in a_{1g}, in the MoO_6 octahedron [11]. As shown in Fig. 1(b), keen competition is present for

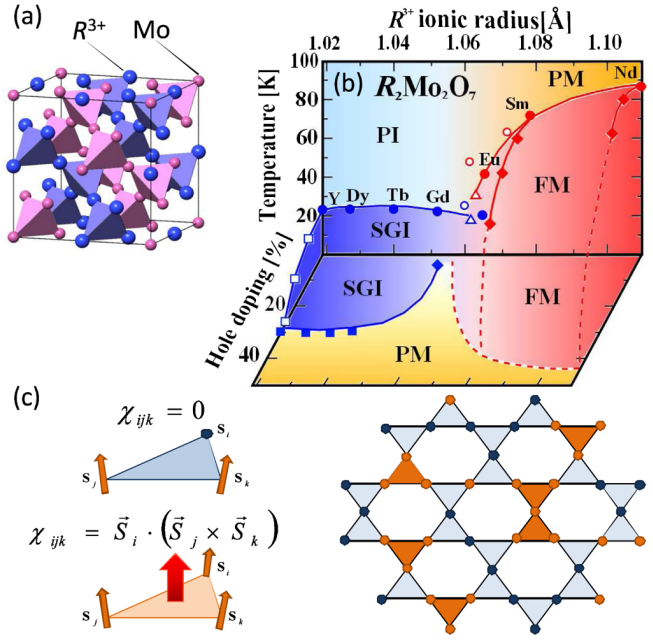

FIG. 1 (color online). (a) Mo and rare-earth-metal ion (R^{3+}) sites in the pyrochlore-lattice structure. (b) The electronic phase diagram for $R_2Mo_2O_7$ with variation of R-site ionic radius and hole doping(Ca or Cd substitutions for A site). PI, PM, SGI, and FM stand for the paramagnetic insulator, paramagnetic metal, spin-glass (Mott) insulator, and ferromagnetic metal, respectively. Solid lines represent the phase boundaries as experimentally determined and dashed lines the expected phase boundaries. (c) Scalar spin-chirality on two-dimensional kagome lattice. It becomes nonzero only when the three neighboring sites are simultaneously occupied by Tb moments.

the ground state between the ferromagnetic metal (FM) and antiferromagnetic insulator; the latter forms the spin-glass state due to the geometrical magnetic frustration on the pyrochlore lattice. Typically in the FM state of $Nd_2Mo_2O_7$, the ferromagnetically ordered spins due to the double-exchange mechanism are slightly (by several degrees [11]) canted with each other via the antiferromagnetic exchange interaction between the Nd moment and Mo $4d$ spin to host the spin chirality. The conduction electron senses such spin chirality in the momentum k space and gains the quantum Berry phase. This is the plausible scenario to explain the large (and unconventional) anomalous Hall effect dominating the low-temperature (< 40 K) response in $Nd_2Mo_2O_7$ [11,12].

In contrast to such a strong-coupling regime with the spontaneous spin chirality and spin polarization, we may seek for the weaker coupling regime [6,7] where the ground state of the conduction electron state remains paramagnetic. Back to Fig. 1(b), the Mott-insulating region with R ion smaller than Gd, the paramagnetic insulator (PI) or lower-temperature spin-glass insulator (SGI), e.g., in $Y_2Mo_2O_7$, can be transformed to the paramagnetic metal (PM) by hole doping or the decrease of the filling of e_g^l electron band [19]. To realize such filling control, we have partly (by 20% or 30%) substituted the Y^{3+} sites with Cd^{2+} ions, in the form of $(Y_{1-y}Cd_y)_2Mo_2O_7$ ($y = 0.2$, 0.3), which causes the Mott transition as expected (see, for example, Fig. 2(b)] [19]. This doping-induced PM phase is analogous to the diffuse PM state realized under high pressures [20], in which the mean free path of the conduction electron is comparable or even less than the atomic spacing (Ioffe-Regel limit). Then, to further introduce the scalar spin chirality that can regulate the conduction electron, we introduce the Ising-moment Tb^{3+} ions [21] on the Y sites, in a form of $(Y_{1-x-y}Tb_xCd_y)_2Mo_2O_7$ ($y = 0.2$, 0.3) with varying concentration x(= 0–0.8, 0–0.7). What we have anticipated is as follows: The Ising Tb moment which directs or counterdirects toward the center of the A site (Y, Cd, or Tb site) tetrahedron couples to the conduction electron and hence plays a role of applying a slanted internal effective magnetic field on the Mo conduction electron. When Tb Ising moments randomly substituting the Y sites can accidentally occupy the three neighboring pyrochlore A sites to have the local spin chirality, the conduction electron moving under an influence of the effective molecular fields from the Tb Ising moment should gain the quantum Berry phase, leading to the topological Hall motion. The situation is schematically

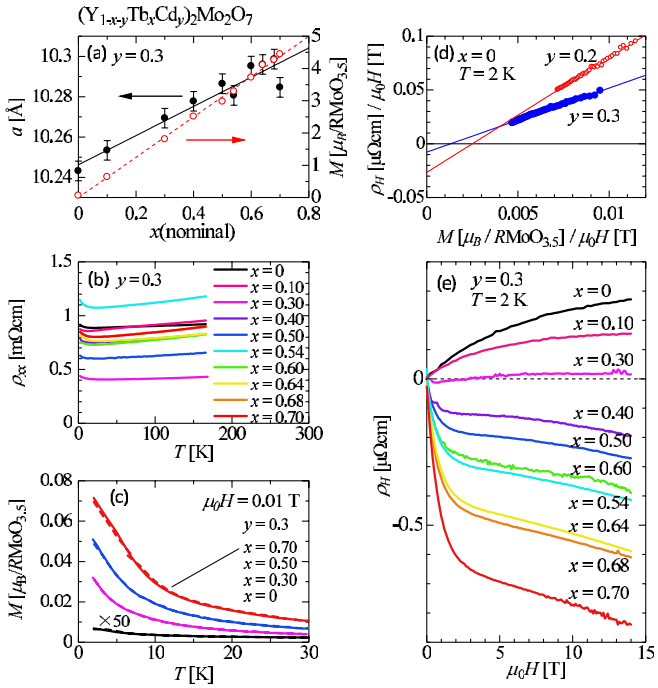

FIG. 2 (color online). (a) The x dependence of lattice constant and magnetization at 14 T in $(Y_{1-x-y}Tb_xCd_y)_2Mo_2O_7$ ($y = 0.3$). (b) Temperature dependence of resistivity ($x = 0$–0.7, $y = 0.3$). (c) Temperature dependence of magnetization in the process of field cool (solid lines) and zero-field cool (dashed lines) at 0.01 T. (d) Plot of the ρ_H/μ_0H vs M/μ_0H relation($x = 0$, $y =$ 0.2 and 0.3). Solid lines are fits by the least-square method. (e) The magnetic-field dependence of Hall resistivity ($x =$ 0–0.7, $y = 0.3$).

drawn as mapped on to the two-dimensional kagome lattice from the actual three-dimensional pyrochlore lattice [Fig. 1(c)]; the marked triangles form the local spin chirality which can endow the conduction electron with the Berry phase. However, the Berry phase does not emerge unless the triad (in the tetragon unit) is occupied simultaneously by three Ising moments [see Fig. 1(c)]. Thus we anticipate controlling the density of the spin-chirality-carrying triad via which the hopping conduction electron can sense locally the Berry curvature.

The pyrochlore compounds $(Y_{1-x-y}Tb_xCd_y)_2Mo_2O_7$ ($x = 0$–0.8; $y = 0.2$, 0.3) were prepared in a polycrystalline form by solid-state high-pressure synthesis. The mixture of respective oxide materials (Tb_2O_3, Y_2O_3, CdO, and MoO_2) and Mo with the prescribed ratio was pressed in the condition of 4.5 GPa and 1200 °C for 20 min. As shown in Fig. 2(a), the magnetization at 14 T, that should be dominated by the field-aligned Tb moments, is linear to the prescribed Tb concentration x; thus the error bar of x is estimated to be less than 0.02. The high-pressure procedure not only promotes the pyrochlore-lattice formation but also keeps the stoichiometry of the compounds with volatile oxides and results in the hard dense sample suitable for the transport measurement. The lattice constant of $(Y_{1-x-y}Tb_xCd_y)_2Mo_2O_7$ ($y = 0.3$) with varying x obeys the Vegard's law as shown in Fig. 2(a), indicating the good solubility of Tb ions to Y sites in the whole region of x [22]. Powder x-ray diffraction measurements indicated that all the samples were single phase. The resistivity was measured with a 4-probe method and the Hall resistivity was measured with a 5-probe method (PPMS, Quantum Design). The magnetization was measured with a SQUID magnetometer (MPMS, Quantum Design).

The paramagnetic metallic state in the hole-doped (Cd-doped) $Y_2Mo_2O_7$ was confirmed in the temperature dependence of resistivity and magnetization (at 0.01 T) for the x(Tb) = 0 compound, as shown in Figs. 2(b) and 2(c), respectively. Even when the Tb moments are doped, the resistivity does not much change; all the resistivities for $x = 0$–0.8 are nearly temperature independent and converging around 0.5–1.0 mΩ cm slightly above the Ioffe-Regel limit value (~ 0.5 mΩ cm) [Fig. 2(b)]. The magnetic susceptibility [Fig. 2(c)] shows the Curie-Weiss like behavior due to the presence of Tb moments, while not showing any trace of the magnetic order. For these compounds, the Hall resistivity (ρ_H) was measured; the magnetic-field (H) dependence of ρ_H at 2 K is shown in Fig. 2(e). With increase of the Tb content x, ρ_H shows a large variation from positive to negative while increasing the absolute magnitude.

Prior to the analysis of ρ_H in terms of possible topological contributions caused by Tb doping, we should first know the ρ_H behavior for Tb-undoped ($x = 0$) metallic compounds, $(Y_{1-y}Cd_y)_2Mo_2O_7$ ($y = 0.2$ and 0.3). As exemplified for ρ_H for $y = 0.3$ in Fig. 2(e), the ρ_H vs H relation shows the upward convex curve, suggesting some anomalous Hall component that comes from the magnetization of Mo spins in addition to the normal Hall effect. The relation is empirically expressed with the normal and anomalous Hall coefficients, R_0 and R_S,

$$\rho_H = R_0 H + R_S M. \quad (1)$$

We plot the $\rho_H/\mu_0 H$ vs $M/\mu_0 H$ relation in Fig. 2(d) for $y = 0.2$, 0.3 ($x = 0$; i.e., no Tb moment). The both compounds well obey the relation (1); the slope stands for R_S, and the intersection at $M/\mu_0 H = 0$ for R_0. The relatively small R_0 values for these metallic compounds are consistent with typical metal values with a large Fermi surface. The larger R_S value for $y = 0.2$ than for $y = 0.3$ may indicate its proximity to the magnetic insulator phase. Hereafter, we take the working hypothesis that these R_0 and R_S values remain unchanged when the Tb^{3+} species are doped on the pyrochlore A site. This assumption is plausible, since the isovalent exchange between Y^{3+} and Tb^{3+} with comparable ionic radii on the pyrochlore A sites does not change the band filling and hence perhaps the Fermi surface area of the PM state. Little sensitivity of the resistivity (ρ_{xx}) to the doped Tb content x as shown in Fig. 2(b) ensures this premise.

With this assumption, we can deduce the topological component of Hall resistivity (ρ_H^T) as the deviation of the observed ρ_H from that of the $x = 0$ compound (as expressed by Eq. (1)). The results for $y = 0.3$ are plotted in Fig. 3(a). The absolute magnitude of ρ_H^T appears to steeply increase with x, while the H-induced M value is proportional to x. On the other hand, the H dependence of ρ_H^T resembles the magnetization curve shown in Fig. 3(c). This is also seen in the ρ_H^T vs M plot shown in Fig. 3(b). However, the change of the ρ_H cannot be interpreted in terms of the effective increase of the magnetization of Mo under the presence of the Tb moment. This is because the ρ_H^T shows the opposite sign (negative) to ρ_H (positive) or its anomalous Hall component $R_S M(>0)$ for the Tb-undoped ($x = 0$) compound, and also because the x dependencies of M and ρ_H^T are totally different (see below).

At least up to the magnetic field of 1.5 T, the value of ρ_H^T is well proportional to M. The measured sample is polycrystalline and the crystal axes are randomly oriented; while the Tb moment shows the Ising anisotropy directing toward the center of A-site tetrahedron, the alignment of Tb moments needs some field value, typically 2–3 T [see Fig. 3(c)]. In this magnetization process, the topological Hall effect is nearly proportional to H or M, as shown in Fig. 3(b). (In the high magnetic-field regime, the opposite-sign contribution of the spin chirality from the 3-in 1-out like Tb-tetrahedron becomes appreciable in increasing the Tb content x, as discussed later.) Here, we plot the values of M and ρ_H^T at $\mu_0 H = 1.5$ T for the $y = 0.2$ and 0.3 compounds as a function of x in Fig. 4. The M value is totally determined by the field-aligned value of the Tb

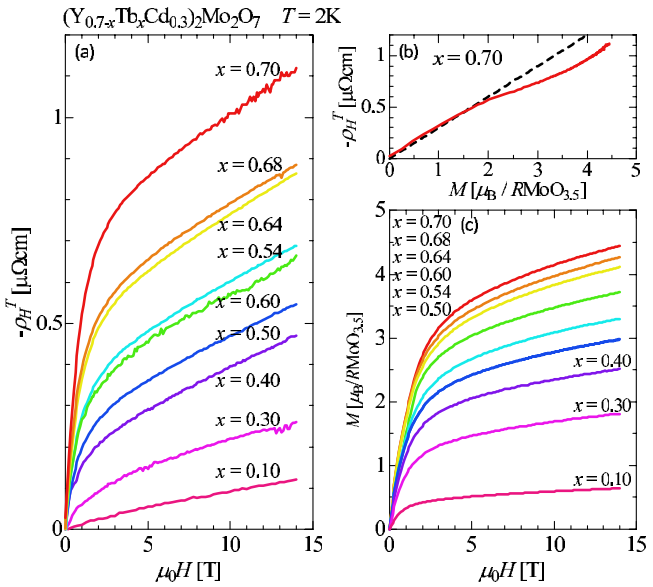

FIG. 3 (color online). (a) The magnetic-field (H) dependence of topological Hall resistivity (ρ_H^T) ($x = 0$–0.7, $y = 0.3$). (b) The magnetization (M) dependence of topological Hall resistivity (ρ_H^T) ($x = 0.7$, $y = 0.3$). (c) The magnetic-field dependence of magnetization (M) ($x = 0$–0.7, $y = 0.3$).

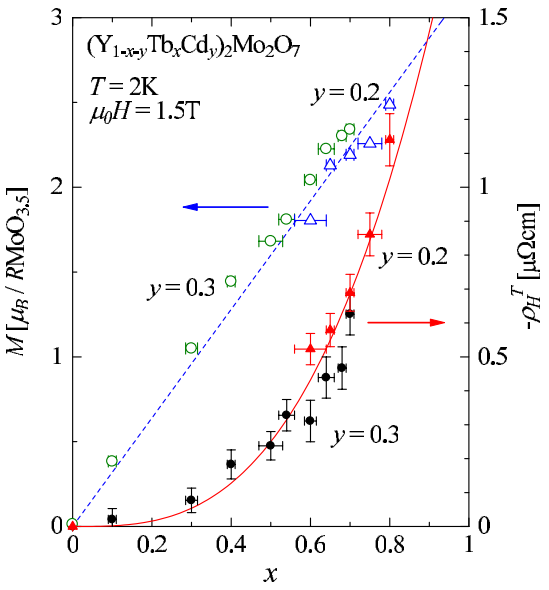

FIG. 4 (color online). The x dependence of topological Hall resistivity (●: $y = 0.3$ and ▲: $y = 0.2$) and magnetization (○: $y = 0.3$ and △: $y = 0.2$) at $\mu_0 H = 1.5$ T. The horizontal error bar for x is estimated from the magnetization data at 14 T in Fig. 1(a). Dashed and solid lines represent the references proportional to x and x^3, respectively.

moment (least affected by the Mo spin polarization) and hence in proportion to Tb content x, as shown with a straight line in Fig. 4. By contrast, the ρ_H^T value increases superlinearly with x; it appears to be approximately represented by the x^3 dependence (the solid curve in Fig. 4). The behavior is in accord with the scenario of the topological Hall effect induced by the scalar spin chirality; the scalar spin chirality represents the three-spin correlation, $\boldsymbol{S}_i \cdot (\boldsymbol{S}_j \times \boldsymbol{S}_k)$, and hence becomes nonzero only when the three neighboring sites are simultaneously occupied by the Tb moments (see the right panel of Fig. 1(c)]. As for the conduction electron propagating on the Mo sublattice, it feels the fictitious magnetic flux B_{eff} (Berry curvature) when the three sites out of the four neighboring A sites are occupied by the Tb moments. Thus, the spin-chirality density, and hence the topological Hall effect, increases with x^3, as observed. The B_{eff} can be deduced from the observed ρ_H^T and $\mu_0 R_0$ (ρ_H/H in the limit of $H \to 0$) values. At $x(\text{Tb}) = 0.70$ and $y(\text{Cd}) = 0.3$, for example, $\mu_0 R_0 \sim 0.01\ \mu\Omega\,\text{cm/T}$ [see Fig. 2(d)] and $\rho_H^T \sim 0.5\ \mu\Omega\,\text{cm/T}$ at $\mu_0 H = 1$ T (or $\sim 1\ \mu\Omega\,\text{cm}$ at $\mu_0 H = 10$ T). This means $B_{\text{eff}} \sim 50$ T (100 T), corresponding to 50 times (10 times) amplification of applied external field B action.

It is worth to note here that the observed THE is also sensitive to temperature. The spin-flipping dynamics via thermal agitation should reduce the spin chirality; in fact we have observed that the topological Hall resistivity steeply decreases as temperature is increased from 2 K; above 20 K it is decreased to less than $1/3$ of the 2 K value. Another important modification from the simple spin-chirality model is seen in the THE in the high-x and high-H regime. As noted in Fig. 3(b), the ρ_H^T value for $x = 0.70$ is nearly proportional to M but above $M = 2\mu_B/R\text{MoO}_{3.5}$ tends to deviate from the linear increase (dashed line in Fig. 3(b)]. This might be ascribed to the onset of the contribution from the all-Tb-occupying-tetrahedron with the 3-in 1-out Ising moment configuration when the applied field is nearly along the [111] direction of some polycrystalline grains. The sign of spin chirality and hence of the Berry curvature are reversed between the 2-in 2-out and 3-in 1-out configurations of the Ising moment [11]. In the case of $Nd_2Mo_2O_7$ crystal, when the strong magnetic field (> 10 T) is applied along the [111] direction, the 2-in 2-out spin configuration is observed to be gradually turned into the 3-in 1-out one, leading to the reduction and then to the sign reversal of spin-chirality-induced anomalous Hall effect [11,12]. The similar reduction of ρ_H^T might occur in the high-field region of this topological Hall system when the density of the all-Tb-tetrahedron becomes appreciable in a high-x region. In fact, the non-negligible deviation (reduction) of the THE from the simple x^3 scaling curve was observed for the high-field (e.g. 14 T) value of ρ_H^T in a high x (e.g. >0.5) region (not shown). Conversely, we may neglect the negative-sign contribution from the 3-in 1-out configuration in such a low field as 1.5 T (Fig. 4), in which the hypothesis of only three-spin (not four-spin) correlation, i.e., the x^3 scaling, works well.

In conclusion, we have succeeded in producing the paramagnetic metallic state in pyrochlore-lattice Mo

oxides with varying density of local spin chirality. The real-space Berry curvature arising from the coupling with the local spin chirality can give rise to the topological Hall effect, being distinct from the both normal (Lorentz force) and spin-orbit-coupling induced anomalous terms. The magnitude of the topological Hall effect is approximately scaled with the cube of the Tb-moment density, ensuring the important role of the three-spin correlation in giving rise to the scalar spin chirality. While this system is in a regime of weak spin-charge coupling, the field alignment of spin chirality amplifies the action of the external magnetic field by more than an order of magnitude in comparison with the normal Hall term. This may suggest possible application of the spin-chirality notion in spin-related electronic technology.

We thank N. Nagaosa for enlightening discussions. This work was partly supported by Grants-in-Aid for Scientific Research (No. 22740220, 20340086, and 22014003) from the MEXT of Japan and FIRST Program by the Japan Society for the Promotion of Science (JSPS).

*Present address: Institute for Materials Research, Tohoku University, Sendai 980-8577, Japan.

[1] N. Nagaosa and Y. Tokura, Phys. Scr. **T146**, 014020 (2012).
[2] S. W. Cheong and M. Mostovoy, Nature Mater. **6**, 13 (2007).
[3] Y. Tokura and S. Seki, Adv. Mater. **22**, 1554 (2010).
[4] N. Nagaosa J.Sinova, S. Onoda, A. H. MacDonald, and N. P. Ong, Rev. Mod. Phys. **82**, 1539 (2010).
[5] J. Ye, Y. B. Kim, A. J. Millis, B. I. Shraiman, P. Majumdar, and Z. Tešanović, Phys. Rev. Lett. **83**, 3737 (1999).
[6] M. Onoda, G. Tatara, and N. Nagaosa, J. Phys. Soc. Jpn. **73**, 2624 (2004).
[7] G. Tatara and H. Kawamura, J. Phys. Soc. Jpn. **71**, 2613 (2002).
[8] P. Bruno, V. K. Dugaev, and M. Taillefumier, Phys. Rev. Lett. **93**, 096806 (2004).
[9] D. Xiao, M.-C Chang , and Q. Niu Rev. Mod. Phys. **82**, 1959 (2010).
[10] K. Ohgushi, S. Murakami, and N. Nagaosa, Phys. Rev. B **62**, R6065 (2000).
[11] Y. Taguchi, Y. Oohara, H. Yoshizawa, N. Nagaosa, and Y. Tokura, Science **291**, 2573 (2001).
[12] Y. Taguchi, T. Sasaki, S. Awaji, Y. Iwasa, T. Tayama, T. Sakakibara, S. Iguchi, T. Ito, and Y. Tokura, Phys. Rev. Lett. **90**, 257202 (2003).
[13] Y. Machida, S. Nakatsuji, Y. Maeno, T. Tayama, T. Sakakibara, and S. Onoda, Phys. Rev. Lett. **98**, 057203 (2007).
[14] S. Mühlbauer, B. Binz, F. Jonietz, C. Pfleiderer, A. Rosch, A. Neubauer, R. Georgii, and P. Böni, Science **323**, 915 (2009).
[15] X. Z. Yu, Y. Onose, N. Kanazawa, J. H. Park, J. H. Han, Y. Matsui, N. Nagaosa, and Y. Tokura, Nature (London) **465**, 901 (2010).
[16] M. Lee, W. Kang, Y. Onose, Y. Tokura, and N. P. Ong, Phys. Rev. Lett. **102**, 186601 (2009).
[17] A. Neubauer, C. Pfleiderer, B. Binz, A. Rosch, R. Ritz, P. G. Niklowitz, and P. Böni, Phys. Rev. Lett. **102**, 186602 (2009).
[18] N. Kanazawa, Y. Onose, T. Arima, D. Okuyama, K. Ohoyama, S. Wakimoto, K. Kakurai, S. Ishiwata, and Y. Tokura, Phys. Rev. Lett. **106**, 156603 (2011).
[19] S. Iguchi, Y. Kumano, K. Ueda, S. Kumakura, and Y. Tokura, Phys. Rev. B **84**, 174416 (2011).
[20] S. Iguchi, N. Hanasaki, M. Kinuhara, N. Takeshita, C. Terakura, Y. Taguchi, H. Takagi, and Y. Tokura, Phys. Rev. Lett. **102**, 136407 (2009).
[21] H. Cao, A. Gukasov, I. Mirebeau, P. Bonville, and G. Dhalenne, Phys. Rev. Lett. **101**, 196402 (2008).
[22] N. Hanasaki, K. Watanabe, T. Ohtsuka, I. Kézsmárki, S. Iguchi, S. Miyasaka, and Y. Tokura, Phys. Rev. Lett. **99**, 086401 (2007).